Archives of Hydro-Engineering and Environmental Mechanics
Vol. 59 (2012), No. 1–2, pp. 37–48
DOI: 10.2478/v10203-012-0003-3

VERSITA

Wind Influence on the Formation of Nearshore Currents in the Southern Baltic: Numerical Modelling Results

Andrei Sokolov, Boris Chubarenko

Institute of Oceanology of Russian Academy of Sciences, Atlantic Branch, pr. Mira, 1, Kaliningrad 236000, Russia, e-mails: ans@smtp.ru (corresponding author), chuboris@mail.ru

(Received November 03, 2011; revised February 22, 2012)

Abstract

A two-dimensional numerical model was used for a simulation of vertical average longshore currents generated by both wind friction and wind-wave action in the nearshore zone. The modelling domain includes the southern part of the Baltic Proper (all boundaries were closed). Wind, uniform in space and varying in time, was the only forcing in the model. The correlation coefficient higher than 0.8 was obtained by model calibration versus the field measurements of currents conducted at the Lubiatowo field station (southern Baltic) during about 1.5 months in 2006. Comparative simulations of total currents including both wind-induced drift and wave components, and of total currents including only a wind-induced drift component, showed that the input of the drift component into currents in the nearshore zone is greater than commonly believed. Wind-induced drift strongly dominates outside the zone of wave transformation, and its input into the total resulting currents remains noticeable even in a zone between the shoreline and the depth of the first wave breaking. Thus, wind-induced drift constitutes up to 50% of the resulting longshore currents for longshore winds and no less than 20% of the longshore component of currents for winds at 45 degrees to the longshore direction.

Key words: currents, waves, numerical modeling, coastal zone, the Baltic Sea

1. Introduction

Currents in a water column are driven by external forces, among which wind-induced forces are some of the most significant ones. There are two main mechanisms of the transformation of momentum from wind forcing to translational water motion. First, wind produces water motion in the surface layer of a water column directly: wind generates tangential stress which causes wind drift currents. Second, wind generates waves, which in their turn cause the wave-induced input into translational water motion. When waves approach the beach at some angle, the momentum induced by wave breaking generates longshore currents that flow parallel to the beach inside the breaker zone (Longuet-Higgins 1970). It is important to note that the term "a longshore current" is usually understood (e.g. Massel 1989) as a wave-induced current. In this paper,

the adjective "longshore" refers exclusively to the direction of the current, irrespective of the mechanism of its formation.

It is traditionally assumed (e.g. Shadrin 1972, Massel 1989) that currents in the breaker zone at an open shore are caused mainly by wind-generated waves and their transformation, whereas the wind drift component may be neglected. Owing to the mutual interaction of all processes in the nearshore zone, the case study approach seems preferable for the examination of this assumption: the roles of wind-induced drift and wind-wave generated current should be considered not in general, but in a specific case of real bathymetry and wind forcing. The hypothesis is that the contribution of wind-induced drift to the resulting currents in the nearshore zone may be comparable with that of wind waves.

The aim of the present study is to examine the particular input of drift- and wave-induced components into the resulting currents in the nearshore zone of a non–tidal sea on the example of the south shore of the Baltic Sea. This shore has an open sandy beach varying in width from 15 to 60 m. The cross-shore bottom profile is characterised by a gentle slope of about 1–2% of steepness (Ostrowski et al 2010b). The sand median diameter is 0.2–0.25 mm.

It is hardly possible to reveal the separate influence of these two components of currents in field measurements (Chao et al 2008), and numerical modelling is the only tool to do that. In this paper, the MIKE 21/3 Coupled Model FM (MIKE 21/3, 2005), developed at the Danish Hydraulic Institute, was used for simulations. This model makes it possible to simulates the mutual interaction between waves and currents, using a dynamic coupling between the Hydrodynamic Module and the Spectral Wave Module, and therefore makes it possible to estimate drift and wave parts of the current separately.

The MIKE 21/3 Coupled Model FM was calibrated versus field measurement data. Then, series of quasi-stationary modelling solutions for constant wind directions were obtained. The comparison of (i) simulations by the coupled model taking into account the interaction of waves and currents, and (ii) simulations for drift currents only, provided data for the estimation of the separate contributions of drift and waves to the resulting currents.

Even though the current structure in the nearshore zone is fully three-dimensional, we have used a 2D mode of the MIKE 21/3 Coupled model FM as a first approximation to study longshore currents. Irrespective of the wind direction, cross-shore currents always accompany the longshore flow (Pruszak et al 2008) and are significantly variable in the vertical direction. Moreover, they may be of the opposite direction in surface and bottom layers. Therefore, a 2D vertically integrated approach is not applicable to the study of cross-shore currents. The possibility of a 2D approach to longshore current simulations is shown in a number of papers (e.g. Longuet-Higgins 1970, Ding et al 2003).

2. Method

2.1. Basic Equations

Basic equations for the MIKE hydrodynamic module in a 2D mode are the shallow water equations (MIKE Sci. Doc. 2005):

$$\frac{\partial h}{\partial t} + \frac{\partial h\bar{u}}{\partial x} + \frac{\partial h\bar{v}}{\partial y} = hS, \tag{1}$$

$$\frac{\partial h\bar{u}}{\partial t} + \frac{\partial h\bar{u}^2}{\partial x} + \frac{\partial h\bar{v}\bar{u}}{\partial y} = f\bar{v}h - gh\frac{\partial \eta}{\partial x} - \frac{gh^2}{2\rho_0}\frac{\partial \rho}{\partial x} + \frac{\tau_{sx}}{\rho_0} - \frac{\tau_{bx}}{\rho_0} + \frac{\partial}{\partial x}(hT_{xx}) + \frac{\partial}{\partial y}(hT_{xy}), \tag{2}$$

$$\frac{\partial h\bar{v}}{\partial t} + \frac{\partial h\bar{u}\bar{v}}{\partial x} + \frac{\partial h\bar{v}^2}{\partial y} = -f\bar{u}h - gh\frac{\partial \eta}{\partial y} - \frac{gh^2}{2\rho_0}\frac{\partial \rho}{\partial y} + \frac{\tau_{sy}}{\rho_0} - \frac{\tau_{by}}{\rho_0} + \frac{\partial}{\partial x}(hT_{xy}) + \frac{\partial}{\partial y}(hT_{yy}). \tag{3}$$

Here, t is the time; x and y are the Cartesian co-ordinates; h is the total water depth; η is the surface elevation; u and v are the velocity components in the x and y direction; f is the Coriolis parameter; g is the gravitational acceleration; ρ is the density; ρ_0 is the reference density; τ_{sx}, τ_{sy} are the wind stresses; τ_{bx}, τ_{by} are the bottom stresses.

The overbar indicates a depth-averaged value.

The lateral stresses T_{ij} include viscous friction, turbulent friction and differential advection. They are estimated by an eddy viscosity formulation based on the depth-averaged velocity gradients:

$$T_{xx} = 2A\frac{\partial \bar{u}}{\partial x}, \quad T_{xy} = A\left(\frac{\partial \bar{u}}{\partial y} + \frac{\partial \bar{v}}{\partial x}\right), \quad T_{yy} = 2A\frac{\partial \bar{v}}{\partial y}, \tag{4}$$

where A is the horizontal eddy viscosity.

The spectral wave module is based on a wave action density balance equation (MIKE 21 Spectral Wave Module 2005):

$$\frac{\partial N}{\partial t} + \frac{\partial}{\partial x}c_x N + \frac{\partial}{\partial y}c_y N + \frac{\partial}{\partial \omega}c_\omega N + \frac{\partial}{\partial \theta}c_\theta N = \frac{S}{\omega}. \tag{5}$$

Here, N is the action density; t is the time; x, y are the Cartesian co-ordinates; θ is the wave direction; ω is the relative (intrinsic) angular frequency.

The first term in the left-hand side of this equation represents the local rate of change of the action density in time. The second and the third terms represent the propagation of action in geographical space (with propagation velocities c_x and c_y in x- and y-space, respectively). The fourth term represents the shifting of the relative frequency due to variations in depth and current (with propagation velocity c_ω in ω-space). The fifth term represents depth-induced and current-induced refraction (with propagation velocity c_θ in θ-space).

The energy source term S represents the superposition of source functions describing various physical phenomena:

$$S = S_{in} + S_{nl} + S_{ds} + S_{bot} + S_{surf}. \quad (6)$$

Here, S_{in} represents the generation of energy by wind, S_{nl} is the wave energy transfer due to non-linear wave-wave interaction, S_{ds} is the dissipation of wave energy due to whitecapping, S_{bot} is the dissipation due to bottom friction and S_{surf} is the dissipation of wave energy due to depth-induced breaking.

2.2. Numerical Model Setup

Nearshore currents are typically simulated in two stages (e.g. Ostrowski et al 2010a): first, the modeling is performed on a large scale, and then the results are used as boundary conditions for smaller-scale modeling.

In this paper, nearshore currents were simulated directly in one stage with the use of a grid with flexible meshes, covering the southern part of the Baltic Proper (Fig. 1). The mesh size for the open sea was about 5–7 km, and in the vicinity of the field measurements point it was about 100–150 m. The digital topography of the Baltic Sea (Seifert, Kayser 1995, Digital… 2008) was used for the computational domain. All boundaries of the simulation area were closed, and wind was the only driving force in the model. It was assumed that wind measured in Lubiatowo could be uniformly applied in the entire area of simulations.

Other main parameters of the model setup were taken as follows:

- computational time step of 6 s (the maximal possible due to computational stability problems);
- constant water temperature of 10°C (a rather good approximation for October--November, when the calibration field data was obtained);
- constant water salinity of 7 psu (a typical value for the southern part of the Baltic Proper);
- horizontal eddy viscosity in Smagorinsky's formulation (Smagorinsky 1963), with a background value of 0.28 m^2/s.

Calibration parameters are discussed in the next section.

2.3. Calibration and Verification of the Model

The calibration and verification of the model were performed with the use of field data from Oct 1–Nov 22, 2006, collected by the Institute of Hydro-Engineering of the Polish Academy of Sciences (IBW PAN) (Pruszak et al 2008). The field data were obtained with an Acoustic Doppler Current Profiler installed about 200 meters off the shore at a point with coordinates 54.815° North and 17.838° East in the vicinity of the Lubiatowo field station of the IBW PAN. The depth at the point of installation was about 4–4.4 meter. The ADCP measured current velocities at 0.4 and 2.4 meters

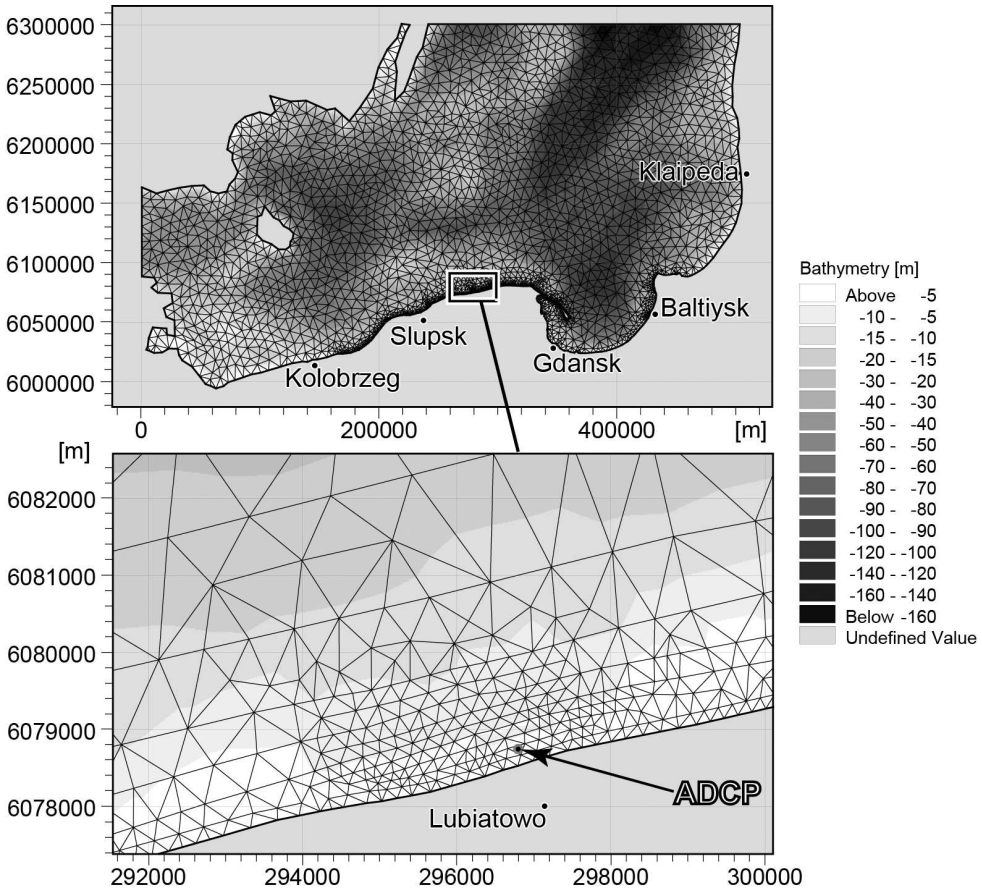

Fig. 1. Computational domain (southern part of the Baltic Proper) and a detailed numerical grid at the Lubiatowo field station, where the ADCP was installed

above the bottom. Wind data were recorded by an automatic meteorological station installed at the Lubiatowo field station of the IBW PAN.

The data from Oct 1–16, 2006, were used for calibration for the following reasons: (a) the current was directed mainly longshore; (b) during this period there were two clear peaks in current velocities related to the increasing wind speed, and current directions during these peaks were opposite; (c) current velocities at 0.4 and 2.4 meters above the bottom were almost identical.

There are several calibration parameters in the MIKE 21 Coupled Model FM. First, and absolutely essential for computational time, is a spatial discretization in the Spectral Wave Module. Test simulations showed that a 24-direction spatial discretization is optimal: the use of more directions produced very similar results but required much more computational time.

The best match of field and simulated current velocities was achieved with the following parameters in the Hydrodynamic Module: (a) Manning number (Gioia and Bombardelli 2002) of 40 $m^{1/3}/s$ for bed resistance; (b) wind friction varying with wind speed: a dimensionless drag coefficient of 0.001255 and 0.002425 for wind speed below 7 m/s and above 25 m/s, respectively, with linear interpolation in-between (MIKE Sci. Doc. 2005). For the Spectral Wave Module, the following parameters were used: (a) 24 directions for Spectral Discretization; (b) a coupled type of air-sea interaction with a background Charnock parameter of 0.01 (Brown and Wolf 2009); (c) wave breaking is included with dimensionless parameters $\alpha = 1$ and $\gamma = 0.8$ (Eldeberky, Battjes 1995, Allard et al 2002); (d) sand grain size of 0.25 mm for the bottom friction model.

Figure 2 presents longshore current velocities: (1) field data, ADCP measurements at a height of 2.4 m above the bottom; (2) a numerical solution with waves (the Spectral Wave Module was used in simulation); (3) a numerical solution without waves (the Spectral Wave Module was disabled, and thus, only the wind drift mechanism of current formation was included). Positive values correspond to eastward transport, and negative to westward transport. Arrows at the top of the picture show the wind speed and direction (the strongest observed wind was 18 m/s). There is a good agreement between curves (1) and (2): typical differences were less than 0.1 m/s and the maximal ones were about 0.2 m/s. Tendencies were well traced – any rise in the measured magnitude of currents was followed by a rise in the model solution. Directions of longshore currents were also in good agreement, e.g. field data from Oct 13–14, 2006, show significant westward currents, and the model solution behaved similarly. A diagram representing the correlation between the field data and simulation results (Fig. 2, insert) demonstrates a principal linear relation for currents higher than 0.2–0.3 m/sec (correlation coefficient of 0.82).

The model was verified with the use of field data from Oct 19–Nov 22, 2006 (Fig. 3). The strongest wind observed during this period was 25 m/s. The field data and simulation results are in rather good agreement except for two periods (Oct 31–Nov 2, and Nov 8, 2006), when significant (up to 1 m/s) westward currents were observed in the field, whereas the wind-driven simulation showed smaller velocities with different directions. This fact could not be explained by local wind action, and was most probably caused by the influence of water movement due to water level oscillations on the scale of the whole Baltic. The correlation coefficient between simulation results and field data for the whole period Oct 19–Nov 22 is 0.64. If the periods Oct 31–Nov 2 and Nov 8, 2006 are excluded from the analysis, the correlation coefficient increases to 0.86.

Calibration and verification results show that the approach applied – computational domain of several hundred kilometers without open boundaries, local wind – gives good results in the nearshore zone of the southern Baltic when currents are mainly wind-driven.

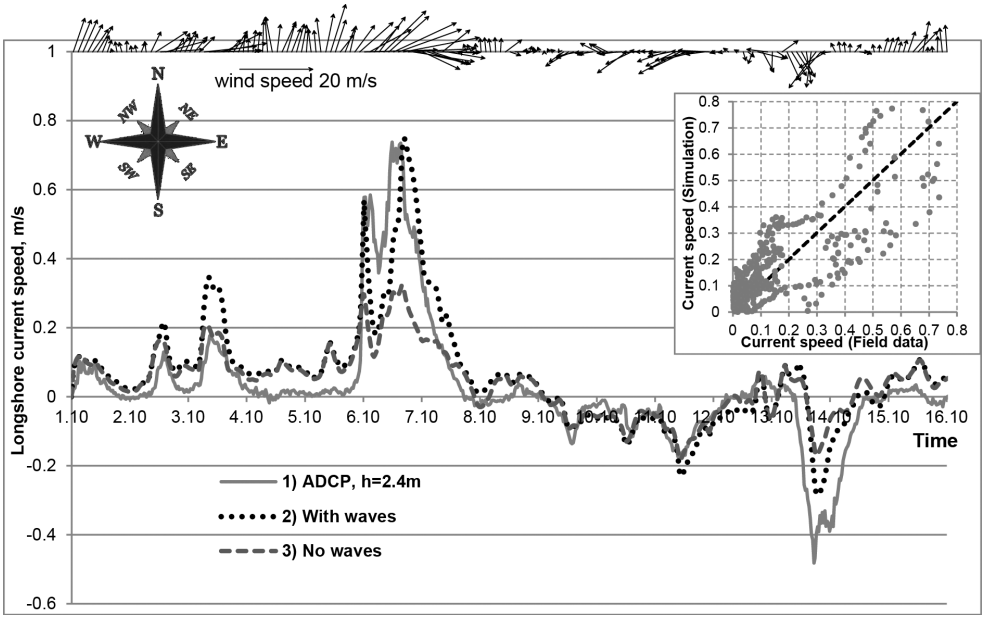

Fig. 2. Longshore current speed, field data and simulation results (Oct 1–16, 2006)

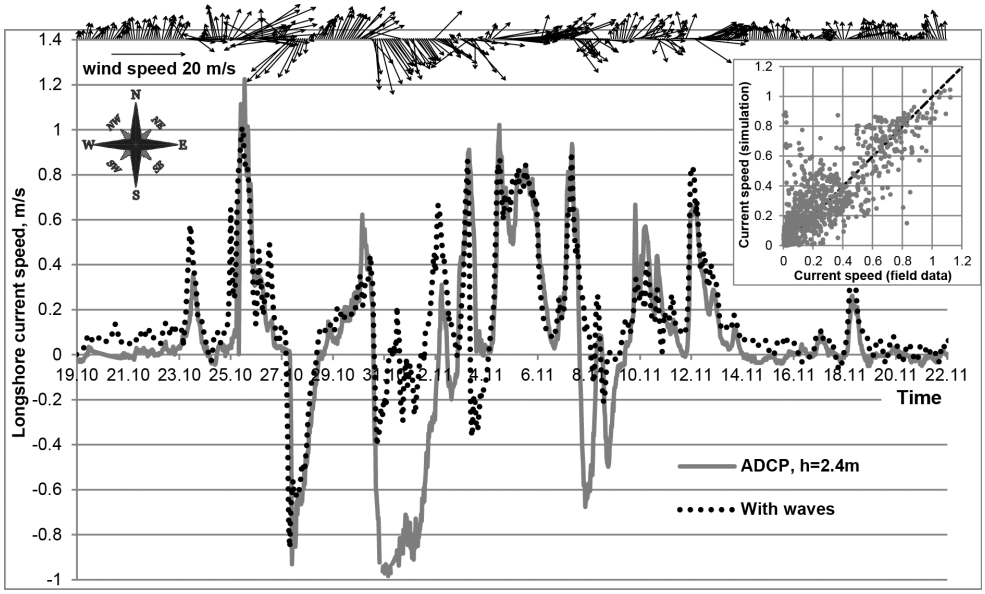

Fig. 3. Longshore current speed, field data and simulation results (Oct 19–Nov 22, 2006)

3. Results

A calibrated MIKE 21 Coupled Model FM was applied to obtain series of steady-state numerical solutions for constant wind forcing (different wind directions and speeds) with an enabled or disabled Spectral Wave Module Drift. For each option, four simulations were run: wind directions W, NW, N, NE; wind speed (Fig. 4) changed stepwise with a time interval of two days[1] from 0 to 18 m/sec with a step of 2.5 m/sec (9 gradations).

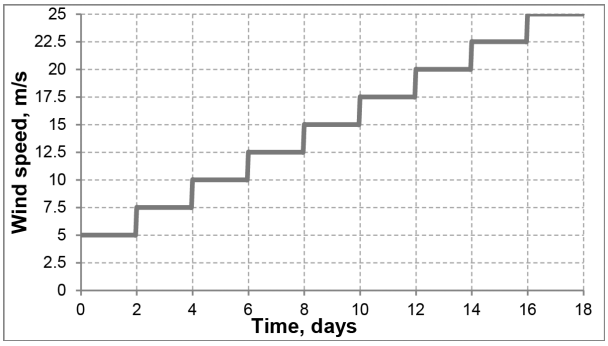

Fig. 4. Model wind speed

Altogether, 72 steady-state current patterns were obtained. An example of depth-averaged current velocity spatial distributions for a west wind of 15 m/s for two options (including wind waves and without them) is shown in Fig. 5. Wave impact on a wind-generated current is noticeable only in a very narrow area between the wave breaking zone and the coastline.

4. Discussion

The results obtained for the calibration period Oct 1–16, 2006, (Fig. 2) showed a significant difference between simulations that took waves into account and those that did not. It was revealed that the wave-driven part of currents at the ADCP location (water depth of about 4.5 m) is negligible if the wind speed is less than 5–7 m/s. The wave-driven part of currents increases along with the wind speed, and for winds higher than 15 m/s the currents simulated with wave input are two or more times larger than those simulated with the wind drift mechanism only.

The steady-state simulation results (Fig. 6) confirmed the above conclusion: wave impact is practically negligible for weak winds (wind speeds of less than 5–6 m/s at the ADCP location). Wave impact increases along with the wind speed, and for winds of 12–15 m/s it exceeds drift impact two, three and even more times, depending on the wind direction.

[1] Preliminary test simulations showed that a two-day simulation period was long enough to achieve a steady-state two-dimensional current pattern near the Lubiatowo field station.

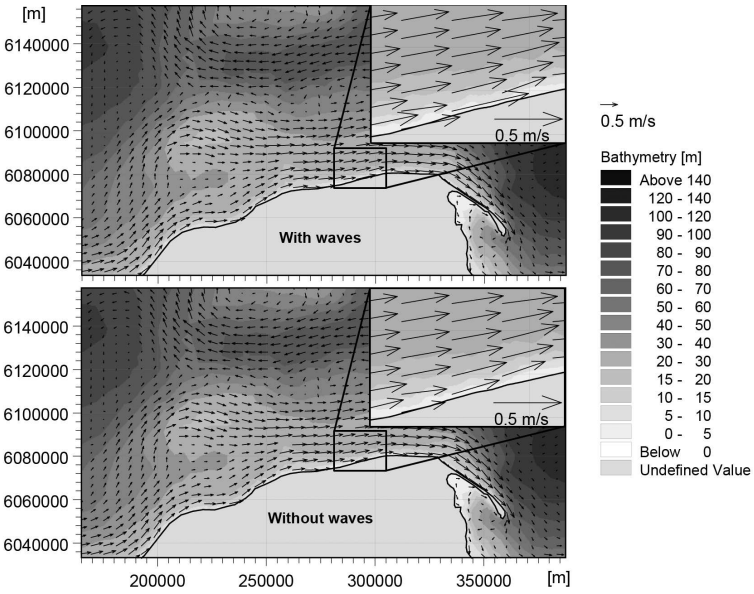

Fig. 5. Depth-averaged flow velocities, calculated with (upper panel) and without (bottom panel) wind waves for a 15 m/s west wind

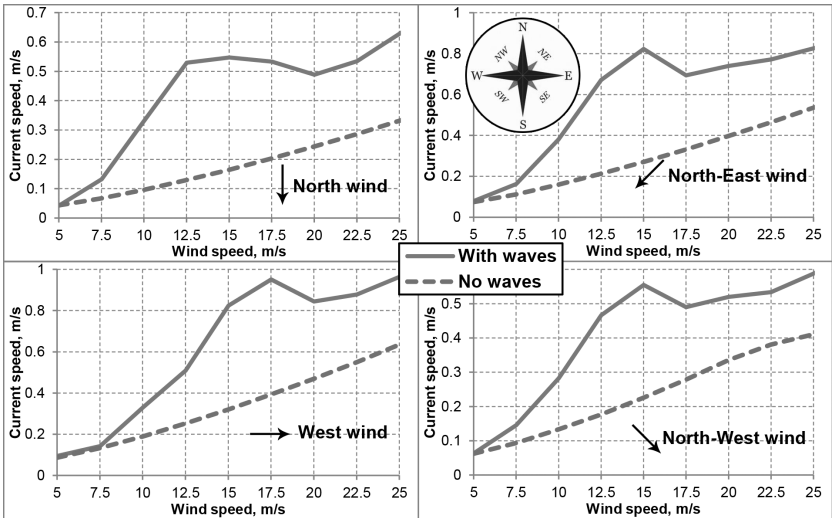

Fig. 6. Simulated speed of steady-state currents (absolute value) at the ADCP location as a function of wind speed, for different wind directions

The following conclusions can be drawn from the relationships presented in Fig. 6. Current velocities are almost linearly dependent on the wind speed if the contribution of waves is ignored, but the relationship becomes essentially non-linear if wave impact

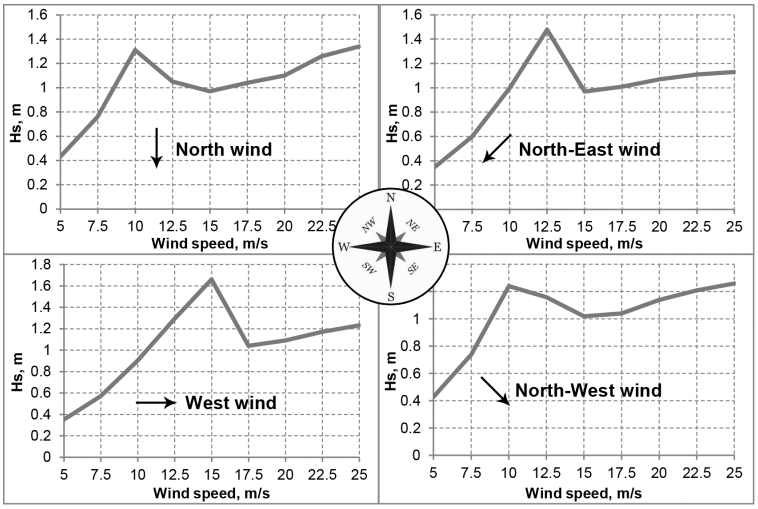

Fig. 7. Significant wave height (H_s) at steady-state conditions at the ADCP location as a function of wind speed, for different wind directions

is included in simulations. The wave height (Fig. 7) increases with the wind speed as well, but decreases significantly after wave breaking. At the ADCP location this happens at a wind speed of 12–17 m/s, depending on the wind direction. A comparison of Figs 6 and 7 shows that the maximum current speed is achieved just after the wave breaking. At the moment of maximum currents, the wave-induced current component 2–4 times exceeds the drift one. It should be noted, however, that drift impact remains quite significant at any wind speed and makes up at least 25–30% of the total current speed.

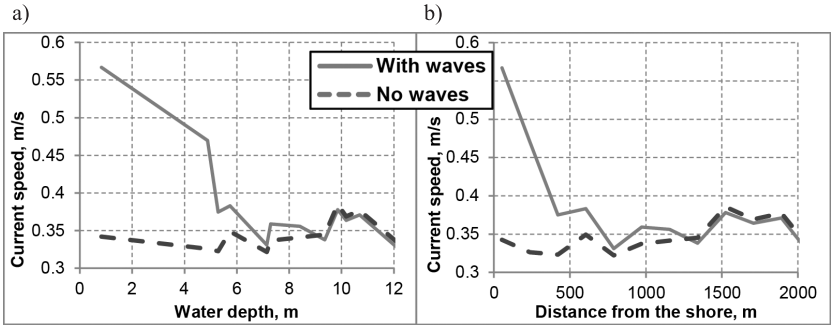

Fig. 8. Absolute values of the speed of simulated steady-state longshore currents for a west wind of 15 m/s

Figure 8 displays the distribution of the longshore current speed (for a 15 m/s west wind) along with the cross-shore profile (at the ADCP location) depending on the water depth (a) and distance from the shore (b). Wave impact is significant in the

coastal strip from the shore to the depth of the first wave breaking. Certainly, the width of this strip depends on the wind speed and direction. For a west wind of 15 m/s, this strip is 600–1000 m wide, extending to the depth of 6–7 m. In deeper areas, the impact of waves on current formation is negligible.

5. Conclusions

1. A two-dimensional model setup (spatial coverage of the southern part of the Baltic Proper only, closed boundaries and a spatially uniform wind obtained at the Lubiatowo field station of the IBW PAN) makes it possible to simulate wind-driven longshore currents in the vicinity of the station with satisfactory accuracy (the correlation coefficient between field measurements and simulations is higher than 0.8).
2. The currents measured during the period Oct 1–Nov 22, 2006, in the nearshore zone at the Lubiatowo field station were mainly wind-driven. There were two time intervals in measurements (Oct 31–Nov 2, 2006, and Nov 8, 2006) when currents were not wind-driven, and therefore, cannot be calculated by the model applied.
3. Wave impact on the longshore current formation is predominant in the zone of wave transformation, especially in the zone between the shoreline and the depth of the first wave breaking.
4. The largest contribution of waves to current formation is observed at depths right behind (landward) the first wave breaker and can reach 60–80% of the total current speed.
5. The contribution of the drift component to the resulting currents is remarkably higher than commonly assumed. The drift component in the total current remains noticeable even in the zone between the shoreline and the depth of the first wave breaking. This component constitutes up to 50% of the observed current for longshore winds and no less than 20% for winds at 45 degrees to the longshore direction. Outside the zone of wave transformation, the wind-induced drift plays the main role.

Acknowledgments

This paper was written during bilateral meetings under the Polish-Russian joint research project “Development of the scientific basis for shore protection of the South Baltic coast” as part of the program of scientific cooperation between the Polish and the Russian Academies of Sciences. The authors are very grateful to Dr. Rafał Ostrowski and Dr. Piotr Szmytkiewicz (both are from the IBW PAN) for the field data that became the basis for the calibration and verification of the model, and for valuable discussions. Dr. Irina Chubarenko’s suggestions on the paper’s content and structure are highly appreciated. The analysis was partly performed with financial support from the Russian Foundation for Basic Research, grant No. 11-05-00674.

References

Allard R., Rogers E., Carroll S. N., Rushing K. V. (2002), *Software Design Description for the Simulating WAves Nearshore Model (SWAN)*, Storming Media, Washington.

Brown J. M., Wolf J. (2009) Coupled wave and surge modelling for the eastern Irish Sea and implications for model wind-stress, *Continental Shelf Research*, **29**, 1329–1342.

Chao X., Jia Y., Shields Jr. E. D., Wang S. S. Y., Cooper C. M. (2008), Three-dimensional numerical modelling of cohesive sediment transport and wind wave impact in a shallow oxbow lake, *Advances in Water Resources*, **31**, 1004–1014.

Digital Topography of the Baltic Sea (2008), The Leibniz Institute for Baltic Sea Research. URL: http://www.io-warnemuende.de/topography-of-the-baltic-sea.html

Ding Y., Wang S. S. Y., Jia Y. (2003), Numerical studies on simulations of waves and nearshore currents in non-orthogonal mesh system, *International Conference on Estuaries and Coasts*, November 9–11, Hangzhou, China, 719–726.

Eldeberky Y., Battjes J. A. (1995), Parameterization of triad interactions in wave energy models, *Proceedings Coastal Dynamics 95*, September 4–8, Gdansk, Poland, IBW PAN, 140–148.

Gioia G., Bombardelli F. A. (2002), Scaling and Similarity in Rough Channel Flows, *Physical Review Letters*, **88**, 014501-1 – 014501-4.

Longuet-Higgins M. S. (1970), Longshore Currents Generated by Obliquely Incident Sea Waves, Parts 1 and 2, *Journal of Geophysical Research*, **75** (33), 6778–6801.

Massel S. R. (1989), *Hydrodynamics of Coastal Zones*, Oceanography Series, **48**, Elsevier Science & Technology.

MIKE 21/3 Coupled Model FM (2005), User Guide, DHI Software.

MIKE 21 & MIKE 3 Flow Model FM Hydrodynamic and Transport Module (2005) Scientific Documentation, DHI Software.

MIKE 21 Spectral Wave Module (2005), Scientific Documentation, DHI Software.

Ostrowski R., Pruszak S., Skaja M., Szmytkiewicz M. (2010a), Variability of Hydrodynamic Coastal Processes in the East Part of the Gulf of Gdansk, *Archives of Hydroengineering and Environmental Mechanics*, **57** (2), 139–153.

Ostrowski R., Pruszak S., Skaja M., Szmytkiewicz M., Trifonova E., Keremedchiev S., Andreeva N. (2010b), Hydrodynamics and lithodynamics of dissipative and reflective shores in a view of field investigations, *Archives of Hydroengineering and Environmentals Mechanics*, **57** (3–4), 219–241.

Pruszak S., Szmytkiewicz P., Ostrowski R., Skaja M., Szmytkiewicz M. (2008), Shallow-water wave energy dissipation in a multi-bar coastal zone, *Oceanologia*, **50** (1), 43–58.

Seifert T., Kayser B. (1995), A high resolution spherical grid topography of the Baltic Sea, *Meereswiss. Ber*, (9), 72–88.

Shadrin I. F. (1972), *Coastal currents of on-tidal sea*, Nauka, Moskva (in Russian).

Smagorinsky J. (1963), General Circulation Experiment with the Primitive Equations, *Monthly Weather Review*, **91** (3), 99–164.